Journal of Fluids and Structures (2001) **15,** 845–866
doi:10.1006/jfls.2000.0377, available online at http://www.idealibrary.com on IDEAL®

NUMERICAL STUDIES OF A FREELY VIBRATING CYLINDER IN A CROSS-FLOW

R. M. C. So, Y. Liu, S. T. Chan and K. Lam

Department of Mechanical Engineering, The Hong Kong Polytechnic University Hung Hom, Kowloon, Hong Kong

(Received 3 February 2000; and in final form 28 November 2000)

A numerical method with four different components is used to simulate the flow-induced vibration at the mid-span of a long slender cylinder, simply supported at both ends, and placed in a uniform cross-flow. The incompressible laminar flow, which is assumed to be two-dimensional, is calculated using a finite element method and the cylinder motion is analysed by a two-degree-of-freedom model (or a spring–damper–mass model). The fluid–cylinder interaction is resolved by an iterative time marching method and the calculated time series are analysed by the ARMA technique. The cases examined include stationary as well as freely vibrating cylinders in a cross-flow. In the vibrating cylinder case, resonance and off-resonance situations are considered. Comparisons are made with experimental measurements for stationary cylinders as well as for a freely vibrating cylinder at off-resonance. The reduced velocity examined varies from 3·6 to 9·2, corresponding to a Reynolds number (Re) range of 2000–5000. At least two different mass ratios and two different reduced damping parameters are investigated. The numerical method is capable of replicating the Strouhal number correctly in the Re range investigated. A comparison of the calculated cylinder dynamics with measurements tends to support the results obtained using the present approach. This is true for both stationary and freely vibrating cylinders over the range of parameters considered. Therefore, the present numerical approach can be used to analyse flow-induced vibration problems in the range of parameters investigated, in spite of the fact that the wake flow is three-dimensional and turbulent.

1. INTRODUCTION

A long slender cylinder with simply supported ends vibrating freely as a result of fluid forcing is one of the most basic and revealing problems in the general case of vortex-induced bluff-body fluid–structure interaction. Here, the phrase "simply supported" means that there are no displacement and moment at the supports. As vortices are shed from the cylinder, they induce a periodic lift force at the shedding frequency and a periodic drag force at twice the shedding frequency. The fluctuating forces cause the cylinder to vibrate at a frequency equal to that of the shedding frequency. In turn, the motion of the cylinder affects the vortex shedding. The periodic forces play a very significant role when their frequencies approach the natural frequencies of the different modes of vibration of the combined fluid–cylinder system. When this happens, the cylinder goes into resonance with possible disastrous consequences. In general, fluid damping limits the vibration amplitude. However, the vibration of the cylinder could be so large that it interferes with and controls the flow pattern. The altered flow field, in turn, changes the flow-induced force, and through a nonlinear process, the vibration of the cylinder could increase still further until a limiting behaviour has been reached at resonance (Zhou *et al.* 1999). The numerical modelling of this problem is quite complicated. It involves fluid–structure interaction, transition from

0889–9746/01/060845 + 22 $35.00/0

a laminar boundary layer flow to a turbulent wake flow, even at a rather modest Reynolds number (Re), a three-dimensional wake in spite of a uniform and two-dimensional mean flow, and structural resonance with vortex shedding.

Computational methods used to simulate the flow around bluff bodies can be divided into two broad categories, the grid methods and the grid-free methods. For the grid methods, such as the direct numerical simulation (Newman & Karniadakis 1997; Evangelinos & Karniadakis 1999; Evangelinos *et al.* 2000) and the finite element method (Mittal & Kumar 1999; Mendes & Branco 1999), the Navier–Stokes equations are solved directly. For the grid-free methods, such as the discrete vortex (Zhou *et al.* 1999) and the surface vorticity method (Lewis 1991; Lam & Chan 1998), the flow field is obtained by solving the vorticity transport equation and by invoking the Biot–Savart Law. Besides the direct numerical simulations (DNS), the usual assumption invoked for the other methods is a two-dimensional laminar flow.

Zhou *et al.* (1999) studied an elastic circular cylinder in a two-dimensional cross-flow using the discrete vortex method incorporating the vortex-in-cell technique. The value of Re was kept at 200, similar to that considered by Newman & Karniadakis (1997), and the cylinder motion is modelled by a spring–damper–mass system. The interactions between the fluid and the structure were considered by solving the equations governing the flow field and the structural motions in an iterative way at every time step. Their results show good agreement with those obtained by Newman & Karniadakis (1997) and that fluid damping is responsible for a limit-cycle oscillation behaviour even at, or close to, resonance. At $\mathrm{Re} = 200$, the shed vortices are still laminar. Consequently, the wake remains laminar. Therefore, a laminar formulation is justified. As Re increases, the shed vortices will become turbulent at $\mathrm{Re} = 400$ (Bloor 1964) and the wake will become three-dimensional and will transit to turbulent at higher Re. When this happens, it is not known whether the laminar formulation is still applicable.

Even though the discrete vortex method coupled with the vortex-in-cell technique proves to be quite useful for very low Re, its extension to higher Re is not straightforward. Furthermore, the method cannot be extended to three-dimensional flow without a complete reformulation. Consequently, it serves as a vehicle to seek basic understanding of the fluid–structure interaction physics of two-dimensional flow. As an applied tool, it is not that useful. The surface vorticity method, on the other hand, could be used to calculate flows at higher Re (Lewis 1991; Lam & Chan 1998). However, it is not clear whether the three-dimensional turbulent wake can be replicated by the method. Furthermore, its application to flow-induced vibration problems has not been attempted before.

Newman & Karniadakis (1997) conducted a DNS study of the flow past a freely vibrating cable using the spectral element method. They eliminated the difficulty of a moving mesh by attaching the coordinate axes to the cable. Their simulations were carried out for two- as well as three-dimensional flows at a fairly low Re, not greater than 200. The three-dimensional simulations showed a greater Re dependence than the two-dimensional simulations. Their study focused both on the flow and the hydrodynamic loads induced on the structure and is one of the first studies that deal with the fully coupled problem of flow-induced vibrations on bluff-bodies.

Since then, Evangelinos & Karniadakis (1999) and Evangelinos *et al.* (2000) extended the DNS method to higher Re using a new class of spectral methods suitable for unstructured and hybrid grids. Their approach was fully three-dimensional, but was limited to $\mathrm{Re} = 1000$ because the cost of simulating at a higher Re becomes quite prohibitive at present. The emphasis of the Evangelinos & Karniadakis (1999) study was on the wake flow and their results showed a three-dimensional turbulent wake in agreement with that observed by Bloor (1964). On the other hand, Evangelinos *et al.* (2000) examined the effects of the

three-dimensional turbulent wake on the cylinder response. Unfortunately, they did not compare their calculations with measurements because reliable measurements of the dynamic characteristics of a freely vibrating cylinder at this Re were not available.

The finite element method of Mittal & Kumar (1999) and Mendes & Branco (1999) was applied to treat the flow-induced vibration problem up to $\mathrm{Re} = 500$. In their studies, a laminar formulation was invoked and the question of a transitional/turbulent wake was not addressed. Again, a comparison of the structural dynamics with measurements was not presented. However, their calculations managed to reproduce the Strouhal excitation that was characteristic at this Re range. In spite of this success, it is not known whether the laminar approach is capable of giving an accurate estimate of the cylinder dynamics at higher Re, as far as the vibration amplitude, mode shape, etc., are concerned.

Most flow-induced vibration problems involve three-dimensional behaviour and occur at very high Re; therefore, there is a real need to develop a numerical method that can treat these practical problems. Among the numerical methods discussed above, it is clear that the vortex and the DNS methods could not be easily extended at present to three-dimensional flow with high Re. On the other hand, the FEM could easily be extended. The question then is how to justify the laminar formulation for flows with high Re. If the numerical method could correctly predict the dynamic response of the structure so that it could be incorporated into a structural design code to account for the effects of flow-induced forces, it could prove as a useful tool for flow-induced vibration problems. In modelling these problems numerically, it is important to correctly reproduce the major frequencies of vortex shedding or the induced forces. The next requirement is to accurately predict the amplitude of oscillations of the unsteady forces. That way, the structural dynamic response could be estimated with fair accuracy, and the possibility of replicating resonance behaviour would be much enhanced. The ability to resolve the wake flow correctly is, therefore, secondary in these flow-induced vibration problems.

In the subcritical Re range, the mean drag is fairly constant and so is the Strouhal number (Gerrard 1961; Bishop & Hassan 1964; Richter & Naudascher 1976). Furthermore, in this Re range, if the oncoming flow is uniform and laminar, Strouhal excitation still dominates and the cylinder response is Strouhal-like up to $\mathrm{Re} > 10^5$ (So & Savkar 1981). This suggests that a laminar formulation to the flow-induced vibration problem in this Re range could be appropriate, as long as the induced force is Strouhal excitation and its major frequency is identical to the vortex shedding frequency. Another point to note is the assumption of two-dimensional flow in most past formulations. How valid this assumption is in the light of a three-dimensional wake, even at relatively low Re (Bloor 1964; Evangelinos & Karniadakis 1999), needs to be examined. If a two-degree-of-freedom model (2-dof) is invoked for the cylinder dynamics, then the assumption of two-dimensional flow is consistent with the 2-dof model. On the other hand, a three-dimensional flow model has to be assumed if the 2-dof model is relaxed in favor of a beam model.

Up to now, an evaluation of the finite element method (FEM) for the calculation of this relatively simple flow-induced vibration problem at $\mathrm{Re} > 500$ has not been attempted. The present study proposes to examine the viability of an FEM, incorporating mesh remapping to accommodate the moving cylinder boundary, on the calculation of a two-dimensional flow-induced vibration problem at subcritical Re that spans the resonance and the off-resonance condition. It is important to resolve the moving boundary correctly if the flow-induced forces and their subsequent actions on the cylinder are to be calculated with accuracy. A two-dimensional laminar flow and a 2-dof model for the cylinder dynamics are assumed. The objective is to assess the viability of these assumptions in the treatment of an experimental flow-induced vibration problem with a wake flow that is inherently three-dimensional and turbulent. Justifications for this approach are the Strouhal response of the

cylinder and the constancy of the Strouhal number in this Re range. It is, therefore, argued that if these characteristics are reproduced fairly correctly by the FEM with mesh remapping, the cylinder dynamics will also be calculated with fair accuracy. The calculated mean drag coefficient, and the cylinder-displacement time series and its spectral characteristics are thoroughly compared with recent experimental measurements obtained in the Re range of 2000–5000 (So *et al.* 2000).

2. NUMERICAL FORMULATION

In the numerical formulation of a flow-induced vibration problem, four components have to be considered. One component is the flow calculation, another is the structural dynamics evaluation, the third is the assessment of fluid–structure interaction and the fourth is the analysis of the results of the time series thus obtained. In the present study, the FEM with mesh remapping is used to calculate the flow field, a 2-dof model is assumed for the cylinder response, an iterative technique is used to resolve the fluid–cylinder interaction and the ARMA technique is employed to analyse the calculated time series. The various components are described below.

2.1. Finite Element Method (FEM)

2.1.1. *The governing equations*

There are three parts in the FEM, the solution of the governing flow equations, the mesh remapping to account for the cylinder motion and the unsteady force calculations. A schematic view of the problem is shown in Figure 1. A long slender cylinder of diameter D with fixed ends is placed in a cross-flow with a free-stream velocity, U_∞. The cylinder has a large aspect ratio; therefore, the flow over a major portion of its span can be considered two-dimensional. Under this assumption, only one unit length of the cylinder is considered, and therefore a spring–damper–mass system can be used to represent the dynamics of the cylinder. The computational domain is a $25D \times 10D$ rectangular region, the upstream length is $5D$, the downstream length is $20D$, and the cylinder is located at the centreline. The

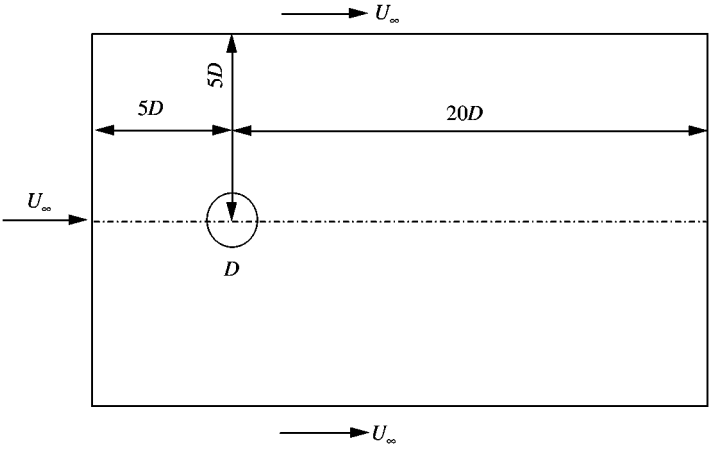

Figure 1. A representation of the finite element calculation domain.

incompressible flow is governed by the laminar Navier–Stokes equations,

$$\nabla \cdot \mathbf{u} = 0, \tag{1}$$

$$\frac{\partial \mathbf{u}}{\partial \tau} + \mathbf{u} \cdot \nabla \mathbf{u} = -\nabla p + \frac{1}{\mathrm{Re}} \nabla^2 \mathbf{u}, \tag{2}$$

where $\mathrm{Re} = U_\infty D/\nu$ is the Reynolds number and ν is the fluid kinematic viscosity. In these equations, $\mathbf{x} = (x, y)$ is the two-dimensional Cartesian position vector, $\mathbf{u} = (u, v)$ is the two-dimensional velocity vector, p is the pressure, τ is time, all dimensionless. The dimensionless variables are defined from the dimensional variables (denoted here by the superscript *, except time t) by $\mathbf{x} = \mathbf{x}^*/D$, $\mathbf{u} = \mathbf{u}^*/U_\infty$, $p = (p^* - p_\infty)/\rho U_\infty^2$, and $\tau = tU_\infty/D$. The formulation of the problem is complete by specifying the boundary conditions as

$$\mathbf{u} = 1, \tag{3}$$

at the upstream far-field, domain top boundary and domain bottom boundary,

$$\frac{\partial \mathbf{u}}{\partial \eta} = 0, \tag{4}$$

at the downstream far-field, and

$$\mathbf{u} \cdot \mathbf{n} = \mathbf{u}_{\mathrm{cy}} \cdot \mathbf{n}, \tag{5}$$

at the cylinder surface. Here, η denotes the normal direction to the boundary, $\mathbf{n}$ is the unit outward normal vector, $\mathbf{u}_{\mathrm{cy}}$ is the velocity vector of the cylinder and the subscript cy denotes the cylinder.

The Navier–Stokes equations are solved using a finite element method and the nonlinear coupling terms in the equations are treated separately, at different fractional time steps, by an operator-splitting time-stepping method. The method is suitable for both steady and transient problems and can readily be extended to include extra equations describing additional physical effects, such as cylinder motion on the flow field and *vice versa* (Bristeau *et al.* 1987).

Using the superscript m to denote the iteration number, the steps involved in generating the solution $\{\theta^{m+1}, \mathbf{u}^{m+1}, p^{m+1}\}$ are as follows:

First fractional step

$$\frac{\mathbf{u}^{m+\delta} - \mathbf{u}^m}{\delta \Delta \tau} - \frac{\alpha}{\mathrm{Re}} \nabla^2 \mathbf{u}^{m+\delta} + \nabla p^{m+\delta} = \frac{\beta}{\mathrm{Re}} \nabla^2 \mathbf{u}^m - (\mathbf{u}^m \cdot \nabla) \mathbf{u}^m, \tag{6}$$

$$\nabla \cdot \mathbf{u}^{m+\delta} = 0. \tag{7}$$

Second fractional step

$$\frac{\mathbf{u}^{m+1-\delta} - \mathbf{u}^{m+\delta}}{(1-2\delta)\Delta \tau} - \frac{\beta}{\mathrm{Re}} \nabla^2 \mathbf{u}^{m+1-\delta} + (\mathbf{u}^{m+1-\delta} \cdot \nabla) \mathbf{u}^{m+1-\delta} = \frac{\alpha}{\mathrm{Re}} \nabla^2 \mathbf{u}^{m+\delta} - \nabla p^{m+\delta}. \tag{8}$$

Third fractional step

$$\frac{\mathbf{u}^{m+1} - \mathbf{u}^{m+1-\delta}}{\delta \Delta \tau} - \frac{\alpha}{\mathrm{Re}} \nabla^2 \mathbf{u}^{m+1} + \nabla p^{m+1} = \frac{\beta}{\mathrm{Re}} \nabla^2 \mathbf{u}^{m+1-\delta} - (\mathbf{u}^{m+1-\delta} \cdot \nabla) \mathbf{u}^{m+1-\delta}, \tag{9}$$

$$\nabla \cdot \mathbf{u}^{m+1} = 0. \tag{10}$$

In the above scheme, α, $\beta \in (0, 1)$ and $\alpha + \beta = 1$, $\delta \in (0, \frac{1}{3})$. The equations at the first and third fractional steps are of the steady quasi-Stokes (QS) problem type, or

$$\alpha_0 \mathbf{u} - \frac{v_1}{\mathrm{Re}} \nabla^2 \mathbf{u} + \delta \nabla p = \mathbf{F}_1. \tag{11}$$

$$\nabla \cdot \mathbf{u} = 0, \tag{12}$$

where $\mathbf{F}_1$ is the body force, $\alpha_0 = 1/\Delta\tau$ and $v_1 = \alpha\delta$. The subproblem at the second fractional step is of the classical nonlinear diffusion–convection problem (NL) type:

$$\alpha_0 \mathbf{u} - \frac{v_2}{\mathrm{Re}} \nabla^2 \mathbf{u} + (1 - 2\delta)(\mathbf{u} \cdot \nabla)\mathbf{u} = \mathbf{F}_2, \tag{13}$$

where $\mathbf{F}_2$ is also a body force and $v_2 = \beta(1 - 2\delta)$. The QS subproblem can be solved by a preconditioned conjugate gradient method, while the NL subproblem can be reformulated as a least-squares problem and solved by a preconditioned conjugate gradient method.

The program development for the solution of these equations was carried out in *Fasttalk* environment, a computer language developed by CSIRO (Stokes 1994). This is a high-level language, consisting of a number of commands to allocate memory, to generate the system matrix for a number of well-known differential operators, and to solve the system of equations. Basic I/O commands are also provided. The actual computation is carried out by *Fastflo*™, another computer language developed by CSIRO. This scheme automatically carries out the assembly and solving processes. The user is free from the routine tasks of implementing the basic finite element blocks; therefore, attention can be concentrated on the algorithm relevant for the governing equations at hand.

Since the cylinder boundary layer is expected to be thin, a fine mesh is concentrated near the cylinder surface. Quadratic triangular elements are used throughout. The number of panels is 220, the number of nodes is about 63 589, and the number of elements is numerically determined to be about 31 589, which is adequate to resolve the velocity and the boundary layers. These numbers are determined by using different meshes, from coarse to progressively finer meshes, until the drag coefficient is mesh-convergent to within a prescribed tolerance (about 0·5%). The wall shear stress τ_w is determined from the calculated boundary layer and the skin friction coefficient, $C_f = 2\tau_w/\rho U_\infty^2$, thus obtained is used to locate the separation angle, θ_s, on the cylinder; θ_s is measured from the front stagnation point. Separation is defined here as the location where C_f goes to zero.

2.1.2. *Mesh remapping*

Solving fluid–structure interaction problems generally involves moving computational domains and dynamic remeshing. With this arrangement, the elastic cylinder is free to vibrate within the flow domain. Therefore, a deforming computational mesh is required to accommodate the arbitrary motion of the elastic cylinder. The cylinder surface is adjusted according to the motion of the cylinder by means of nodal displacement. At each time step, the displacement of the cylinder, which is represented by the position vector $\mathbf{Z}(X/D, Y/D)$, is calculated. In order to distribute the mesh deformation as uniformly as possible, i.e., to minimize local mesh deformation, a Laplacian equation of displacement is solved throughout the computational domain with the cylinder displacement as the boundary condition. This equation is given by

$$\nabla^2 \boldsymbol{\delta} = 0, \tag{14}$$

and the boundary conditions are $\boldsymbol{\delta} = 0$ at the outside boundary and $\boldsymbol{\delta} = \mathbf{Z}$ at the cylinder wall. The entire computational mesh is adjusted by a Laplacian interpolation, which is designed to map a mesh smoothly onto a reasonably similar shape, specified by the displacement of the elastic cylinder. *Fastflo*™ has built-in facilities that allow this mesh remapping procedure to be carried out easily.

2.1.3. *Flow-induced force calculation*

Once the velocity and the pressure field have been calculated, the induced force on the cylinder is determined using the formula,

$$\mathbf{F}(\tau) = \oint \left(-p\mathbf{n} + \frac{1}{\mathrm{Re}} (\nabla \mathbf{u} + \nabla \mathbf{u}^{\mathrm{T}}) \cdot \mathbf{n} \right) (1)\, \mathrm{d}s. \tag{15}$$

The integration is performed around the circumference of the cylinder and over one unit spanwise length. In equation (15), s is the elemental arc length and $\mathbf{n}$ is the outward unit normal of the cylinder. The two-dimensional force vector, $\mathbf{F} = \{F_D, F_L\}$, consists of the dimensionless unsteady drag and lift force. The corresponding coefficients are defined as $C_D = 2F_D/\rho U_\infty^2 D$ and $C_L = 2F_L/\rho U_\infty^2 D$, respectively.

2.2. Cylinder Response

For a long slender cylinder with simply supported ends in a cross-flow, the motion of the cylinder is essentially dominated by vibration along the x- and y-direction only. If mode shape information is not of interest, then the cylinder dynamics can be described by a 2-dof model. Therefore, it is assumed that the circular cylinder is mounted as a spring–damper–mass system, which represents the situation at the mid-span of the long slender cylinder where the vibration amplitude is a maximum. With this approximation, the cylinder motions are described by the 2-dof dynamic equation,

$$\ddot{\mathbf{Z}} + \frac{4\pi\zeta_s}{U_r} \dot{\mathbf{Z}} + \left(\frac{2\pi}{U_r} \right)^2 \mathbf{Z} = \frac{\mathbf{C}_F}{2M^*}, \tag{16}$$

where $\mathbf{Z} = (X/D)\mathbf{i} + (Y/D)\mathbf{j}$, X and Y denote the instantaneous positions of the cylinder in the x- and y-directions, respectively, ζ_s is the dimensionless structural damping coefficient, $M^* = m_{\mathrm{cy}}/(\rho D^2)$ is the mass ratio, ρ is the air density, m_{cy} is the cylinder mass per unit length, $\mathbf{C}_F = 2\mathbf{F}/\rho U_\infty^2 D$, is the force coefficient, $U_r = U_\infty/f_n^* D$ is the reduced velocity and f_n^* is the natural frequency of the stationary cylinder. This is an appropriate choice of characteristic frequency because the natural frequency of the stationary cylinder is well defined. The solution yields the vibration displacement and the velocity of the cylinder as they respond to the flow-induced forces. Since the flow-induced force is the forcing function in equation (16), the incompressible flow solution is coupled with the cylinder response. Therefore, the flow equations and equation (16) have to be solved simultaneously if fluid–structure interactions are to be adequately resolved at each time step. The numerical procedure is described in the next section.

2.3. Fluid–Structure Coupling

In the FEM approach, the reference frame is fixed at the far-field, i.e., the cylinder is free to vibrate within the calculation domain. At each time step, the fluid flow is determined using

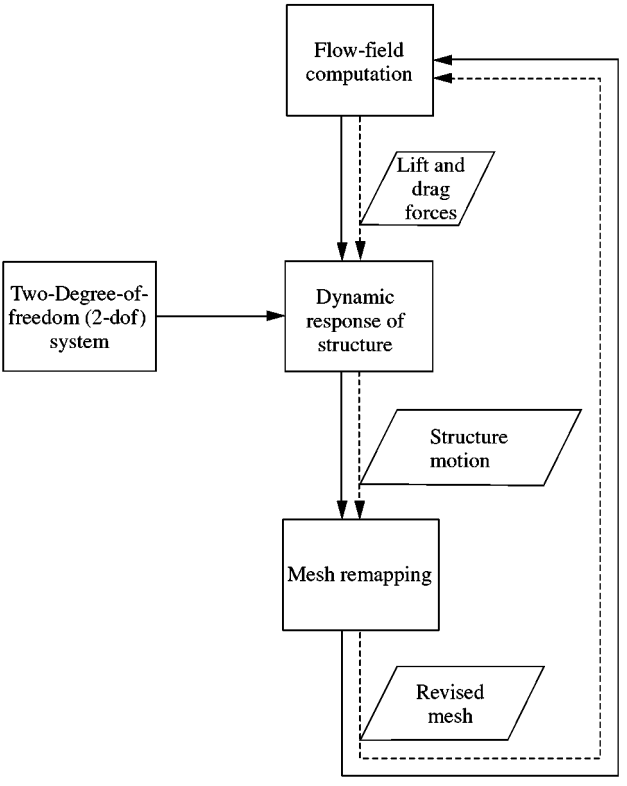

Figure 2. Flow chart illustrating the numerical calculation and fluid–structure coupling.

the FEM method. The force on the cylinder is calculated using equation (15). This is then used as an input to equation (16) and the response of the cylinder is calculated by solving equation (16) using the Runge–Kutta method. The cylinder is moved according to its displacement, and the mesh is remapped according to this motion. Then the flow field is determined again using the new location of the cylinder and its velocity as boundary conditions. In order to account for the fluid–structure interaction properly within each time step, an inner iteration loop is used until a stable status is reached (Figure 2). In such a process, the cylinder motion, the flow field, and the fluid forces are evaluated at the same time at the end of each time step. The dashed (virtual) line in Figure 2 shows this step in the numerical computation. The readers are referred to Jadic *et al.* (1998) for a description of the process.

2.4. Data Analysis

The calculated and measured time series are analysed using the autoregressive moving average (ARMA) technique. Details of the ARMA technique can be found in Mignolet & Red-Horse (1994) to which interested readers are referred. The use of this technique to analyse time series derived from flow-induced vibration problems has been attempted by Jadic *et al.* (1998), Zhou *et al.* (1999) and So *et al.* (1999), and their results had been compared with those deduced from the fast Fourier transform method. The method was found to be able to correctly resolve the spectral characteristics and the effective damping of

the cylinder. Furthermore, ARMA was able to give a more accurate determination of the major frequencies and their associated damping ratios. Therefore, it is more suitable for flow-induced vibration problems (Jadic *et al.* 1998) and is adopted for the present analysis.

Only the stationary part of the signal is used for the analysis. In most of the calculations, stationary behaviour was achieved beyond $\tau = 80$. Therefore, the chosen period for most calculations is $100 \leq \tau \leq 200$. However, in some cases, this chosen period is not long enough and results in fairly large mean values of the lift and transverse displacement. Ideally, the period should be chosen such that the mean values of the lift and transverse displacement are less than 1% of their respective root-mean-square values. In the present study, the period is chosen to yield a mean drag that does not vary by more than 1%.

2.5. Validation and Comparison

The present formulation assumes the cylinder to be infinitely long; hence the spring–damper–mass (or 2-dof) model for the cylinder dynamics can be invoked. In addition, the flow around the cylinder is assumed to be two-dimensional, thus implying that there is a perfect correlation along the span of the cylinder. Therefore, vortex shedding is two-dimensional and this limits the Re range in which the calculations can be carried out and yet the assumptions still remain valid (Evangelinos & Karniadakis 1999). On the other hand, according to So & Savkar (1981), Strouhal excitation is still predominant in spite of the fact that the vortices shed from the cylinder surface and the wake are turbulent. This Strouhal excitation will persist up to $\mathrm{Re} > 10^5$ if the free-stream turbulence level is extremely low. If these assumptions were invoked for flows at higher Re, their validity has to be proven by a comparison with experimental measurements at these high Re. The objective of the present study is to attempt a prediction of the cylinder response correctly; therefore, the ability of the FEM to replicate the Strouhal excitation at these Re is most important.

Among the more suitable experiments that could be used for comparison are those carried out by So & Savkar (1981), Szepessy & Bearman (1992) and So *et al.* (2000). So & Savkar (1981) measured the span-wise averaged force using force cells over the Re range of $\sim 5 \times 10^4$–10^6, while Szepessy & Bearman (1992) used a spatial pneumatic pressure average technique to deduce the sectional average force over the Re range of 8×10^3–$1{\cdot}4 \times 10^5$. On the other hand, So *et al.* (2000) used a laser vibrometer to measure mid-span transverse displacement at Re ranging from 800 to < 5000. The experiments of So *et al.* (2000) were carried out with cylinders having relatively large aspect ratios. Therefore, a two-dimensional flow was established over a large portion of the cylinder, even though the wake is three-dimensional. The experiments of So & Savkar (1981) and Szepessy & Bearman (1992) were carried out at relatively high Re. In order to gain insight into the applicability of the FEM under the two-dimensional laminar assumption, this first attempt is carried out with flows whose Re is less than 5000. Therefore, the following comparison with experiments will only be made with the data of So *et al.* (2000).

Validation of the FEM is carried out in three stages; the first is to assess the viability of the FEM for a stationary cylinder, the second is for a freely vibrating cylinder using the FEM with mesh remapping and the final stage is to verify the numerical calculations with experimental measurements. The calculations of the stationary cylinder in a cross-flow are compared with mean measurements reported in the literature (Roshko 1954; Schlichting 1968) in Section 3. The performance of the FEM with mesh remapping for elastic cylinders over a range of U_r that spans the resonance case is discussed in Section 4. Finally, a detailed comparison of the numerical calculations with the measurements of So *et al.* (2000) for an off-resonance case at $\mathrm{Re} = 3340$ is given in Section 5.

3. STATIONARY CYLINDER

The first comparison between the FEM results and measurements is carried out for the case of a stationary cylinder in a cross-flow. Two cases with Re = 800 and 2500, respectively, are calculated and compared. This choice of Re is intended to cover the sensitive Re range where the mean C_D drops slightly from above 1 to just below 1 (Schlichting 1968). The numerical methods should be able to yield this trend if they are capable of reproducing the flow behaviour properly. The comparisons are made with the separation angle (θ_s) prediction, the mean C_D, $\bar{C}_D$, the calculated C_D and C_L time series and their spectra. The calculated mean C_L, $\bar{C}_L$, is also reported to show the relative error in the numerical calculations. Strictly speaking, $\bar{C}_L$ should be zero. However, its value depends to a large extent on the time period chosen for the overall calculation of the mean values.

The ability of the FEM to predict flow separation on the cylinder is evaluated first by examining the Re = 800 case. Experimentally, the measured mean θ_s occurs at about 80 to $< 90^\circ$ from the front stagnation point for the range $1{\cdot}24 \times 10^3 < \mathrm{Re} < 4 \times 10^4$ (Zdravkovich 1997). The calculated distribution of C_f along the surface of the stationary cylinder at Re = 800 is shown in Figure 3. Since the flow is unsteady, C_f is also time dependent. The three distributions shown in Figure 3 are for the situations where C_f goes to zero at the minimum, mean and maximum angle, respectively. The point at which $C_f = 0$ corresponds to the separation point. Based on this, θ_s thus determined ranges from a minimum of 95° to a maximum of 109°, and the mean angle is about 100·3°. This prediction is consistent with the values reported in Zdravkovich (1997) for the Re range of 174 to ~ 500 but not for higher Re. In view of this, it can be said that FEM over-predicts the mean θ_s. The same is also true for the Re = 2500 case, where the calculated θ_s is similar to that reported for the Re = 800 case. It will be shown below that the inability to predict separation correctly does not affect the calculation of the flow-induced forces and their spectra.

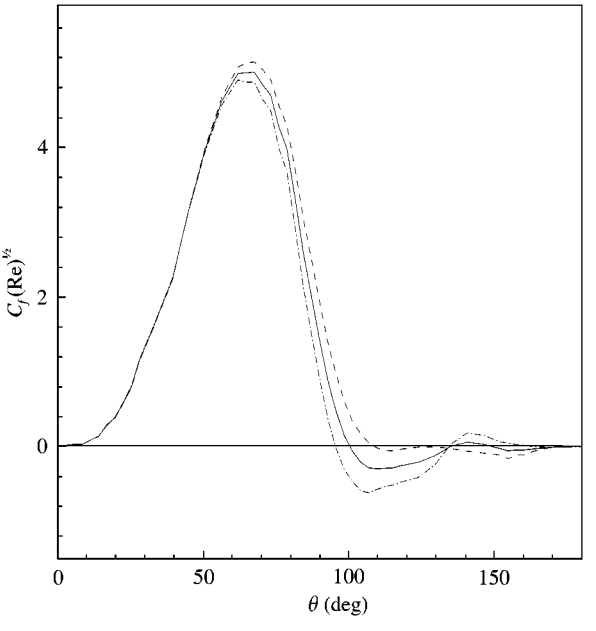

Figure 3. Distribution of the FEM-calculated C_f along the cylinder surface at Re = 800: -----, instantaneous C_f with max θ_s; ——, time averaged C_f; - · - · - · - · -, instantaneous C_f with min θ_s.

The calculated C_D and C_L time series for the Re = 800 case is shown in Figure 4. They show that the induced forces are Strouhal-like with few high frequency components. The calculated statistics for this case is given in Table 1. In addition to the present results, the experimental data collected by Roshko (1954) and Schlichting (1968) at about the same Re are also shown for comparison. The value of $\bar{C}_D$ deduced from the FEM is very close to the experimental data (Schlichting 1968). This good agreement is fortuitous and is not due to the accuracy of the FEM. Strictly speaking, a two-dimensional calculation should yield a $\bar{C}_D$ that is $\sim 5\%$ higher than the measurement. Instead, the present result is about 2% lower (Table 1). Possible reasons for this result are the over-prediction of θ_s, which contributes incorrectly to a smaller wake, the assumption of laminar shed vortices, and the assumption of a two-dimensional laminar wake. The root-mean-square drag coefficient, C'_D, varies from $\sim 10\%$ to $\sim 13\%$ of the root-mean-square lift coefficient, C'_L, depending on the Re. These values seem to be consistent with those reported in the literature (Khalak & Williamson 1996).

Spectra E_L and E_D of C_L and C_D, respectively, for the Re = 800 case are shown in Figure 5. Here, E is the ARMA power spectral density, which is defined as the square norm of the system function scaled by the sampling interval and the white noise variance (Marple 1987). The spectral density E is dimensionless, because the equations solved are nondimensional. Spectrum E_L clearly shows a third harmonic of $\overline{f_s^*}$. A difference in the normalized shedding frequency, $\overline{f_s^*} = \mathrm{St}^* = f_s^* D/U_\infty$, exists between the numerical calculation and the experimental data (Roshko 1954). Here, St* is the Strouhal number of the stationary cylinder. From this point on, the asterisk is used to denote the properties of the stationary cylinder. The FEM under-predicts $\overline{f_s^*}$, and the difference is about 5% (Table 1). Besides $\overline{f_s^*}$ and $3\overline{f_s^*}$ shown in Table 1, the major frequency of the drag signal, $\overline{f_{sD}^*}$, is also determined from its spectrum and listed in the table. It can be seen that, as expected in a Strouhal excitation, the dominant frequency of the drag signal is twice that of the lift. The fact that $\overline{f_{sD}^*}$

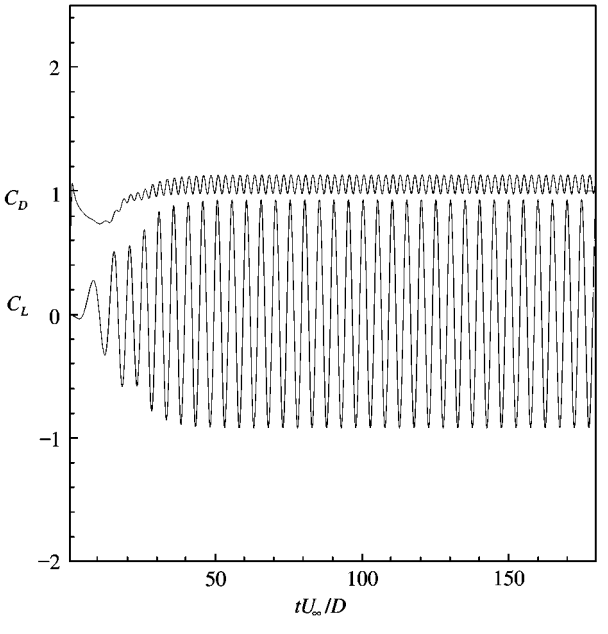

Figure 4. The C_L and C_D time series at Re = 800 for the stationary cylinder.

TABLE 1
Comparison of the FEM calculated characteristics with measurements for a stationary cylinder

	Re = 800		Re = 2500	
	FEM	Measurements	FEM	Measurements
$\bar{C}_D$	1·056	1·08 (Schlichting 1968)	0·9903	0·95 (Schlichting 1968)
C'_D	0·054	—	0·0812	—
$\bar{C}_L$	0·003	—	0·006	—
C'_L	0·651	—	0·6813	—
$\overline{f_s^*}$	0·2002	0·21 (Roshko 1954)	0·2052	0·21 (Roshko 1954)
$\overline{f_{sD}^*}$	0·4029	—	0·4104	—
$3\overline{f_s^*}$	0·6056	—	0·6131	—

does not show up in the lift spectrum simply says that the coupling between the lift and drag direction is very weak at Re = 800. Together, these results show that the excitation is of the Strouhal rather than of the buffeting type.

Comparisons at Re = 2500 are also tabulated in Table 1. At this Re, there is a possibility that the boundary layer on the cylinder surface might become turbulent and this will, in turn, lead to a turbulent separation. However, the major focus is not on this flow behaviour, but rather on the cylinder dynamics, whether it is a Strouhal or a buffeting response. According to the study of So & Savkar (1981), Strouhal excitation was observed up to $Re > 10^5$, where St* was measured to be 0.21. Therefore, it is safe to say that at Re = 2500, the cylinder response should still be Strouhal-like. In this case too, the predicted $\bar{C}_D$ agrees with the experimental data, but it is about 5% higher than the reported measurement. The reason could be that the smaller wake predicted is more representative of the experimental flow at Re = 2500 than at Re = 800. The calculated spectral density clearly shows $\overline{f_s^*}$ and its second and third harmonics. As before, the $\overline{f_{sD}^*}$ determined from the drag spectrum is given in Table 1 and it is twice that of $\overline{f_s^*}$. In this subcritical Re range, St* is quite constant. Therefore, essentially there is no difference in the calculated $\overline{f_s^*}$ in these two Re cases.

Finally, it should be pointed out that the calculated $\bar{C}_L$ for the two Re cases is close to zero, as expected. The value of $\bar{C}_L$ is $< 1\%$ of C'_L. This could be due to a numerical truncation and a possibility that the record length used is not long enough for the cases examined. Therefore, the error could be improved by taking a longer period or sample length in the calculation of $\bar{C}_L$.

The above comparisons show that the FEM is capable of predicting fairly correctly the vortex shedding frequency and the mean drag on the stationary cylinder in the Re range of 800–2500. This suggests that, as far as these mean properties of the stationary cylinder are concerned, the assumption of a two-dimensional laminar wake is quite appropriate. Attempts to verify the C'_L and C'_D calculations were futile because, according to Khalak & Williamson (1996), the scatter in unsteady lift-force data for the stationary cylinder case reported in previous studies is of the order of 400%. Some of these discrepancies could be attributed to the effects of a three-dimensional wake flow (Szepessy & Bearman 1992), while others could be due to a free-stream turbulence (So & Savkar 1981). The next step is to assess how well the FEM with mesh remapping can calculate a freely vibrating cylinder in a cross-flow.

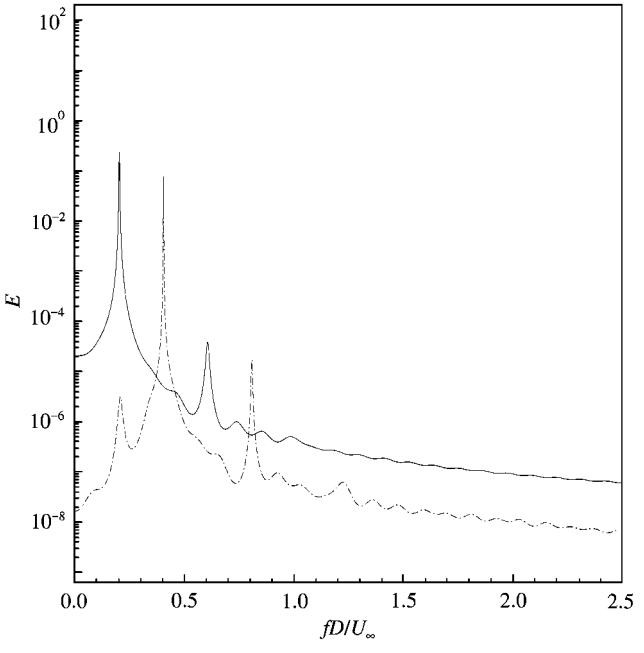

Figure 5. Comparison of E_L and E_D at Re = 800 for a stationary cylinder: ——, E_L; - · - · -, E_D.

TABLE 2
Comparison of the FEM calculated statistics for an elastic cylinder

	$U_r = 3{\cdot}6$ (Re = 2000)	$U_r = 4{\cdot}6$ (Re = 2500)	$U_r = 9{\cdot}2$ (Re = 5000)
$\bar{C}_D$	1·239	1·256	1·40
C'_D	0·0877	0·054	0·186
$\bar{C}_L$	− 0·003	0·008	− 0·020
C'_L	0·835	1·004	1·14
$\bar{Y}/D$	− 0·0008	0·004	− 0·008
Y'/D	0·128	0·258	0·188
$\bar{X}/D$	0·1003	0·1656	0·753
X'/D	0·0046	0·0038	0·0096
$\bar{f}_n$	0·231	0·2127	0·1051
$\bar{f}_s$	0·2122	0·2127	0·2202
$\overline{f_{sD}}$	0·4254	0·4254	0·4354
$3\bar{f}_s$	0·6381	0·6431	0·6557

4. FREELY VIBRATING CYLINDER

Three cases of a long slender elastic cylinder in a cross-flow are examined. The reduced velocities for these cases are selected to be $U_r = 3{\cdot}6$, 4·6 and 9·2, and the corresponding Re are Re = 2000, 2500 and 5000 (Table 2). For all cases, $M^* = 1$ and the reduced damping parameter $S_g = 8\pi^2 \mathrm{St}^{*2} M^* \zeta_s = 1$ are specified. The three cases are selected to bracket the resonance case, which occurs at $U_r = 4{\cdot}6$. Two-dimensional unsteady force measurements at these Re are rather scarce. The measurements of Szepessy & Bearman (1992) were mostly for cylinders with relatively small aspect ratios; therefore, three-dimensional effects rendered their data not very appropriate for a comparison with two-dimensional calculations. This

section attempts to assess the ability of the FEM with mesh remapping to resolve the resonance and off-resonance behaviour of a freely vibrating cylinder in a cross-flow. In the following, the resonance case is discussed first because of the relatively strong nonlinear fluid–structure interaction. Therefore, this case is the most taxing on any numerical methods. If the numerical method cannot resolve the fluid–structure interaction properly, its ability to estimate the vibration characteristics of this resonance case will be greatly diminished.

4.1. Resonance Case ($U_r = 4{\cdot}6$)

In order to illustrate the effectiveness of the mesh remapping technique, the finite element mesh at two different time steps for the resonance case are shown in Figure 6. The finite element mesh at a time step when the cylinder has no displacement is shown in Figure 6(a). Its corresponding mesh at a time step when the cylinder reaches its maximum displacement is displayed in Figure 6(b). It is obvious that the mesh remapping technique is effective in redefining the moving boundary for the flow calculation.

The time series of C_L and Y/D and their corresponding power spectra are shown in Figures 7 and 8, respectively. It can be seen that the C_L and Y/D signals track each other closely and that their spectra yield the same major frequencies. Most important is the coincidence of the shedding frequency, $\bar{f}_s$, with the natural frequency of the combined fluid–cylinder system, $\bar{f}_n$. These frequencies together with the statistics of the C_L, C_D and Y/D signals are tabulated in Table 2. Besides the shedding and natural frequency, the major frequency of C_D and the higher harmonics determined from the spectrum of C_L are also shown in Table 2 for comparison. It can be seen that $\overline{f_{sD}^*}$ is twice that of $\bar{f}_s$ and the only higher harmonics discernible is the third. These results clearly show that the induced force and the cylinder response are Strouhal-like.

The calculated $\bar{C}_D$ is about 30% larger than that given by the stationary cylinder at the same Re, while the C'_D is $\sim 35\%$ smaller (cf. Tables 1 and 2). On the other hand, the C'_L is $\sim 65\%$ larger. As a result, the C'_L/C'_D ratio increases from 8 for the stationary case to about 20 for the resonance case. The effect of cylinder vibration on the induced forces is very significant. This is also reflected in the y displacement, where Y'/D is about $\frac{1}{4}$. In terms of the major frequencies, the present numerical method is capable of resolving them; at least demonstrating clearly that, at resonance, $\bar{f}_s$ and $\bar{f}_n$ are identical. Again, the calculated $\bar{C}_L$ is

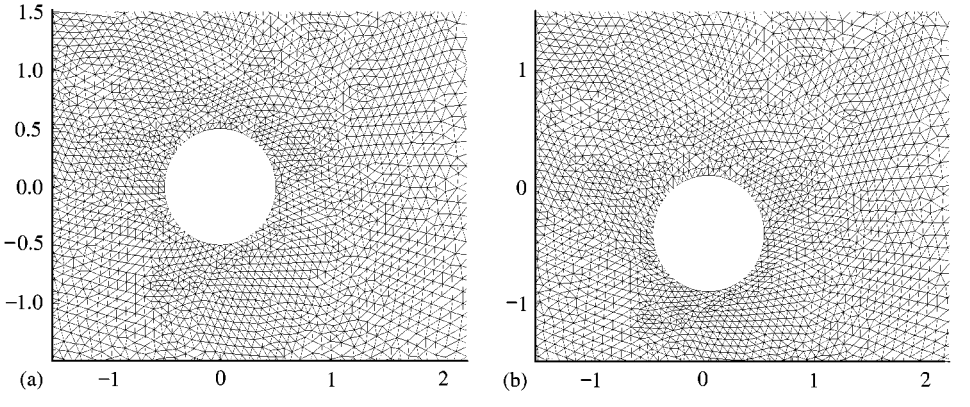

Figure 6. Computational mesh distribution with and without cylinder displacement for a freely vibrating cylinder.

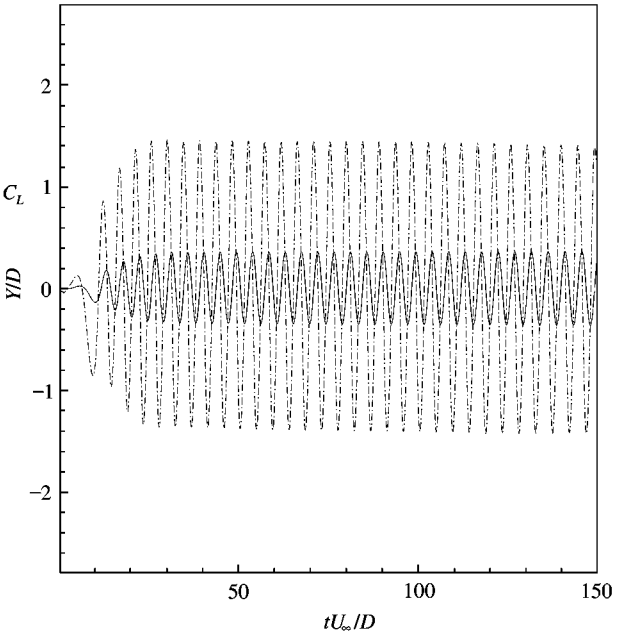

Figure 7. The C_L and Y time series at $U_r = 4{\cdot}6$ (Re = 2500) for a freely vibrating cylinder: ——, Y/D; - · - · -, C_L.

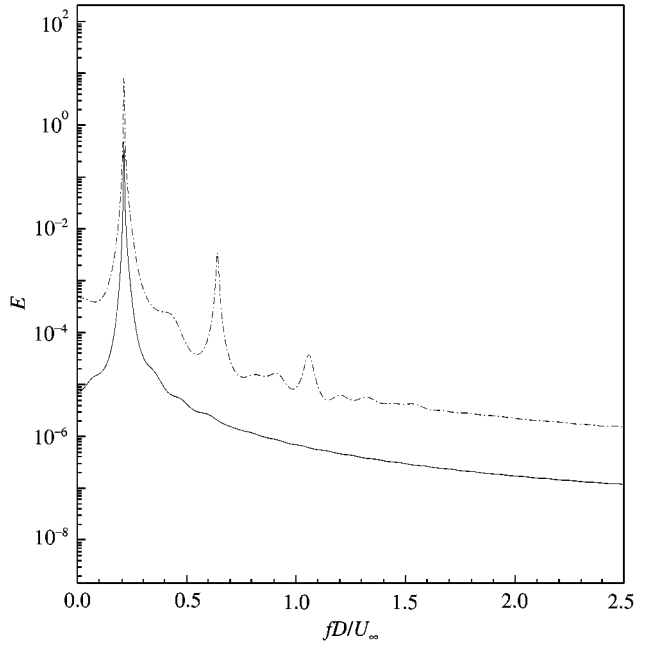

Figure 8. Comparison of E_L and E_Y at $U_r = 4{\cdot}6$ (Re = 2500) for a freely vibrating cylinder: ——, E_Y; - · - · -, E_L.

nonzero and, in this case, it is also $< 1\%$ of C'_L. As pointed out in Section 3, numerical truncation errors and an insufficiently long record length could give rise to a very small value for $\bar{C}_L$.

4.2. Off-Resonance Cases ($U_r = 3{\cdot}6$ and $9{\cdot}2$)

The C_L time series of these two cases are shown in Figure 9, the corresponding Y/D time series in Figure 10 and the power spectra of C_L and Y/D for the case $U_r = 9{\cdot}2$ are plotted in Figure 11 for comparison. Statistics of the different signals and the major frequencies determined from their spectra are tabulated in Table 2 for comparison. From these results, the following observations can be made. The numerical method is capable of resolving $\bar{f}_s$ and $\bar{f}_n$ and the variation of $\bar{f}_n$ with U_r. It is obvious that U_r has a very significant effect on $\bar{f}_n$; a reduction of more than 50% in $\bar{f}_n$ is noted when U_r increases from 3·6 to 9·2. However, the effect on $\bar{f}_s$ is minimal. In fact, the noted variation is within the numerical error margin. The calculated $\bar{f}_s$ for the three cases considered is about the same. This seems to verify the fact that the Strouhal number does not vary much in this range of Re. The calculated $\bar{C}_D$ also bears this out because it is approximately the same for the three Re considered.

The correctness of these calculations has to be validated against measurements; otherwise, the viability of the FEM with mesh remapping cannot be demonstrated. Furthermore, the assumption of a two-dimensional laminar wake flow for a freely vibrating cylinder still needs to be verified. These points are addressed in the next section.

5. COMPARISON WITH MEASUREMENTS

A rather elaborate experiment on the flow-induced vibration of a long slender cylinder has been carried out (So *et al.* 2000). Thus, the flow over a major portion of the cylinder span is two-dimensional in spite of the fact that the wake flow might be three-dimensional. In this sense, the flow at mid-span is close to that modelled by the present numerical approach. Two cases were examined in detail; one was a resonance case while another was an off-

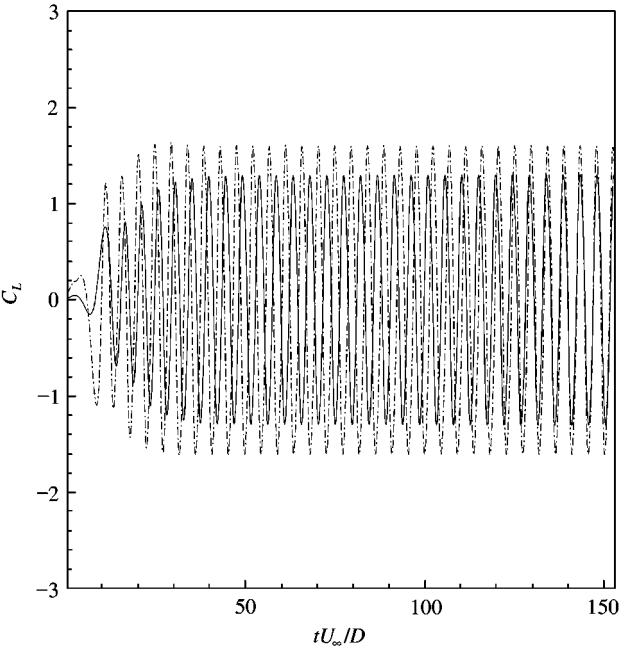

Figure 9. Comparison of the C_L time series at $U_r = 3{\cdot}6$ and $9{\cdot}2$ (Re = 2000 and 5000) for a freely vibrating cylinder: ——, $U_r = 3{\cdot}6$; - - - - - - - -, $U_r = 9{\cdot}2$.

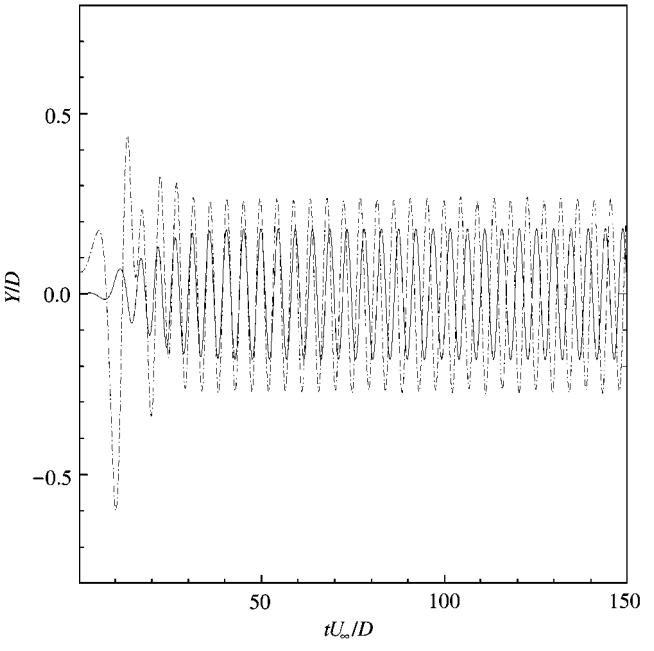

Figure 10. Comparison of the Y/D time series at $U_r = 3{\cdot}6$ and $9{\cdot}2$ (Re = 2000 and 5000) for a freely vibrating cylinder: ——, $U_r = 3{\cdot}6$; - · - · - · -, $U_r = 9{\cdot}2$.

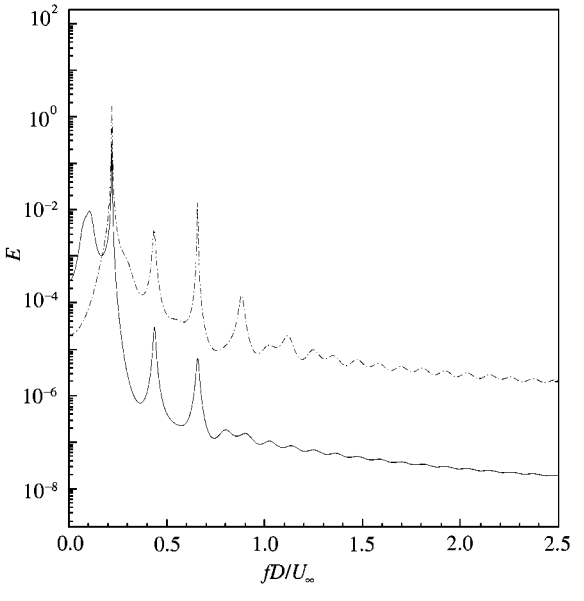

Figure 11. Comparison of E_L and E_Y at $U_r = 9{\cdot}2$ (Re = 5000) for a freely vibrating cylinder: - · - · -, E_L; ——, E_Y.

resonance case. In order to verify the ability of the numerical techniques to predict $\overline{f}_n$ and $\overline{f}_s$, an attempt is made here to compare the numerical calculations with the off-resonance case, where $\overline{f}_s$ and $\overline{f}_n$ are distinctly present in the measured Y/D signal (So *et al.* 2000).

All experiments were carried out in a suction-type wind tunnel. The length of the square test section (0·35 m × 0·35 m) was 0·5 m. A circular cylinder with $D = 6$ mm was mounted in the mid-plane of the test-section at a location that was 20 cm downstream of the test-section entrance. This gives an aspect ratio of 58 for the test cylinder, thus justifying it as a long slender cylinder. The cylinder was mounted to simulate a fixed–fixed end support. Thus, the cylinder deflection at the support is essentially zero. This arrangement allows the 2-dof assumption (or spring–damper–mass system) to be made in the structural dynamics. Various materials, such as acrylic, bronze, glass and steel, were used to fabricate the cylinder. The experiments were carried out with particular values specified for U_r and M^*, and the calculations were performed using the same U_r and M^*. The U_∞ could be varied from a low of about 2 m/s to a high of ~ 26 m/s. The corresponding Re varied from 800 to 9000, and M^* is estimated to be 445 for an acrylic cylinder. The free stream turbulence intensity was measured at 0·5%. A range of U_r was investigated, covering situations close to resonance to far away from resonance. The case where $U_r = 15{\cdot}0$ and $\mathrm{Re} = 3340$ was investigated in detail with measurements made along the span of the cylinder. However, the present comparison is made with measurements obtained at mid-span only. The reduced damping parameter for this case is $S_g = 8\pi^2 \mathrm{St}^{*2} M^* \zeta_s = \sim 41$. Thus, $M^* = 445$ and $S_g = \sim 41$ are substantially different from those specified in Section 4. In addition to comparing the measured Y/D and its statistics, an attempt is also made to compare ζ_e, the effective damping ratio, which is the sum of ζ_s and ζ_f, the fluid damping ratio. That way, the ability of the numerical methods to yield damping information can also be assessed. The ARMA data analysis technique is used to determine the damping ratio following the procedure proposed by Zhou *et al.* (2000). The calculated and measured statistics are shown in Table 3.

It can be seen that the calculated $\bar{C}_D$ agrees to within 1·3% with the measurement (Table 3). The reasons for the good agreement are similar to those given in the case of the stationary cylinder. This result is consistent with those reported in Sections 3 and 4 for the stationary and vibrating cylinders and lends support to the suggestion that the incorrect prediction of the separation angle does not seriously affect the calculation of $\bar{C}_D$. A comparison of the calculated Y/D time series of the cylinder with the experimentally measured time series in the stationary region of the signal is shown in Figure 12. The calculated and

TABLE 3
Comparison of the calculated and measured statistics at $U_r = 15$ and $\mathrm{Re} = 3340$

	$U_r = 15$ (Re = 3340)	
	FEM	Experiment
$\bar{C}_D$	0·968	0·955
C'_D	0·092	—
$\bar{C}_L$	0·007	—
C'_L	0·710	—
$\bar{Y}/D$	0·000006	—
Y'/D	0·00050	0·00048
$\bar{X}/D$	0·0062	—
X'/D	0·000039	—
$\bar{f}_n$	0·075	0·075
$\bar{f}_s$	0·212	0·216
$\overline{f_{sD}}$	0·424	—
$3\bar{f}_s$	0·6366	0·6533
ζ_e	0·0369	0·0314

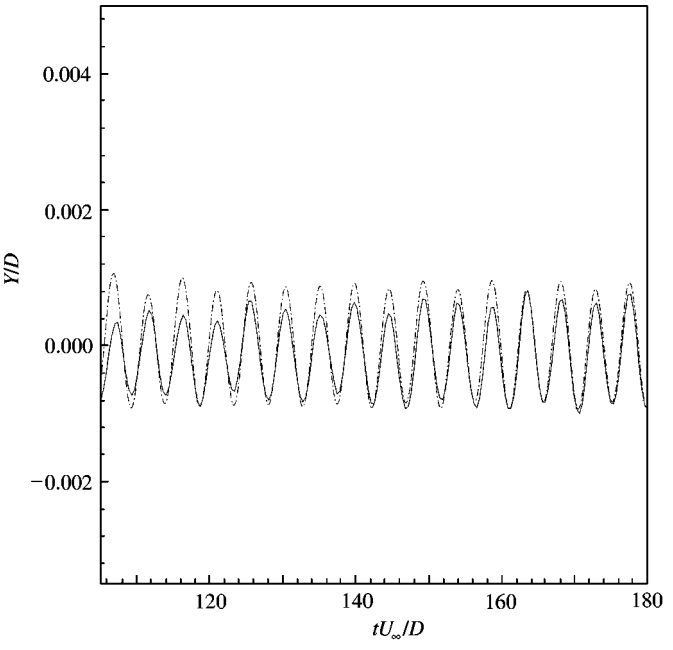

Figure 12. Comparison of the calculated and measured Y time series at $U_r = 15$ (Re = 3340): ——, Measured; - · - · - ·, FEM.

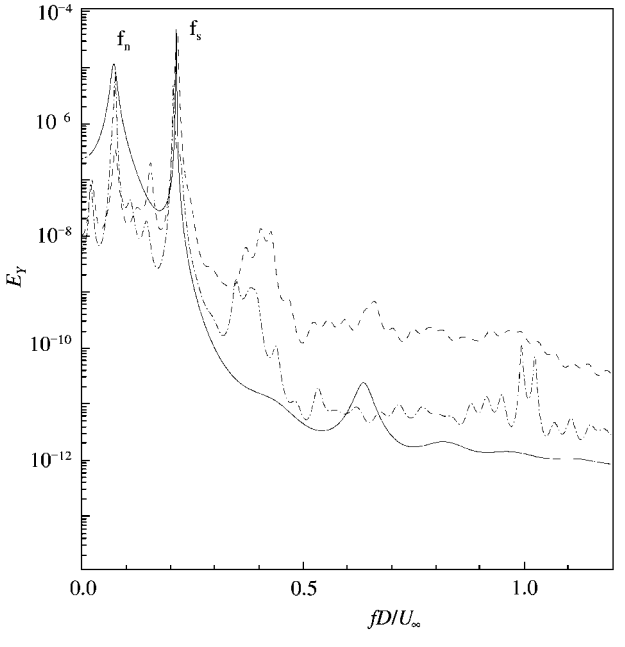

Figure 13. Comparison of the calculated and measured power spectral density E of Y/D at $U_r = 15$ (Re = 3340): - · - · - ·, $(E_Y)_m$ filtered; ———, $(E_Y)_c$ calculated; -----, $(E_Y)_m$ measured.

the measured signal track each other rather well. The measured Y'/D is 0·00048, while the correspondingly calculated value is 0·00050. This yields an error of about 4%. These discrepancies could be partially attributed to the neglect of fluid damping in equation (16).

The calculated spectrum of Y/D, $(E_Y)_c$, is compared with the measured spectrum, $(E_Y)_m$, in Figure 13. The difference between $(E_Y)_c$ and $(E_Y)_m$ at lower frequencies could be attributed to wind tunnel noise contamination. If $(E_Y)_m$ is calculated from a signal that filters out the low-frequency content, i.e., passing the measured signal through a high-pass filter set at 30 Hz, the agreement between the calculated and measured spectrum at high frequency is much improved (Figure 13). The agreement in the major frequencies between the calculation and measurement is excellent, the fluid–structure natural frequencies are exactly the same, the difference in major shedding frequency is about 2%, and even the difference in the third harmonic is only 2·5% (Table 3). At this U_r, the cylinder vibrates at a frequency far away from $\bar{f}_n$. That is why the $\bar{f}_s$ value thus determined is three times larger than $\bar{f}_n$. The coupling between X/D and Y/D is very weak. As a result, $\overline{f_{sD}}$ cannot be detected from the measured Y/D signal. The value of $\overline{f_{sD}}$ listed in Table 3 is determined from the drag signal. This further indicates that the FEM method is capable of resolving fluid–structure interactions correctly, at least in the prediction of the major frequencies in Y/D. The Y/D signal is used to determine the damping ratio. Only the damping ratio associated with $\bar{f}_n$ is used for the comparison, because this is the frequency where the calculated and measured signals are in complete agreement (Table 3). The calculated ζ_e from the FEM signal is in fair agreement with the measurement, the error being about 17% (Table 3).

Taken together, all these results show that the FEM with mesh remapping is a viable method for flow-induced vibration modelling at the subcritical Re range considered.

6. CONCLUSIONS

In any flow-induced vibration problem, there are four components to the numerical calculation. The first is flow analysis, the second is the calculation of the structural dynamics, the third is the technique used to evaluate the fluid–structure interaction and the fourth is the data analysis method. This paper makes an attempt to evaluate the viability of the finite element method (FEM) with mesh remapping for flow calculation under the assumption of two-dimensional and laminar wake flow in flow-induced vibration problems.

The vehicle to achieve this is a relatively simple flow-induced vibration problem, a long slender cylinder with fixed ends freely vibrating in a cross-flow. That way, a laminar two-dimensional approach can be assumed for the flow. Consistent with this assumption, a 2-dof model is used to describe the cylinder dynamics. An iterative time marching technique is used to determine the fluid–cylinder interaction at every time step. Data analysis is carried out using the ARMA technique. The validation is made in three different stages; stationary cylinder at two values of Re, vibrating cylinder at three values of U_r bracketing the resonance situation, and detailed evaluation against the experimental measurements for an off-resonance situation. In all these cases, the Re values were chosen so that they were within the subcritical range, 800–5000. For the vibrating cases, different values of M^* and S_g are investigated. Thus, the validation is fairly comprehensive in that it covers a rather wide range of the parameters of importance in flow-induced vibration problems.

The FEM gives an incorrect calculation of the mean separation angle for the stationary case and the prediction is off by more than 18%. In spite of this, the calculated $\bar{C}_D$ is in good agreement with the measurement and so is the predicted vortex shedding frequency. For the vibrating cylinder case, the FEM with mesh remapping is capable of correctly predicting the Strouhal response in the Re range investigated. Furthermore, it is equally capable in its handling of the resonance and off-resonance case over a range of cylinder mass ratio, reduced velocity and reduced damping factor. The calculated Y/D time series, $\bar{f}_s$ and its

harmonics, and $\bar{f}_n$ are in good agreement with the measurements. Therefore, it can be concluded that, even though the FEM gives an incorrect prediction of the mean separation angle, it is a viable method to use for resolving flow-induced vibration problems at these sub-critical Re, U_r, M^* and S_g considered. This is in spite of the assumption of a two-dimensional flow and a laminar wake for problems where the wake flow is inherently three-dimensional and turbulent. Therefore, these results suggest that the key to the numerical modelling of a flow-induced vibration problem is the ability of the numerical techniques to resolve the fluid–structure interaction, so that the induced forces and their major frequencies are calculated correctly.

ACKNOWLEDGEMENTS

The Support given by the Research Grants Council of the Government of the HKSAR under Grant Nos. PolyU5159/97E and PolyU5128/98E and by The Hong Kong Polytechnic University under Central Research Grant No. G- V396 is gratefully acknowledged.

REFERENCES

BISHOP, R. E. D. & HASSAN, A. Y. 1964 The lift and drag forces on a circular cylinder in a flowing fluid. *Proceedings of the Royal Society* **A277,** 51–75.

BLOOR, M. S. 1964 The transition to turbulence in the wake of a circular cylinder. *Journal of Fluid Mechanics* **19,** 290–304.

BRISTEAU, M. O., GLOWINSKI, R. & PERIAUX, J. 1987 Numerical methods for the Navier–Stokes equations: applications to the simulation of compressible and incompressible viscous flows. *Computer Physics Reports* **6,** 73–187.

EVANGELINOS, C. & KARNIADAKIS, G. E. 1999 Dynamics and flow structures in the turbulent wake of rigid and flexible cylinders subject to vortex-induced vibrations. *Journal of Fluid Mechanics* **400,** 91–124.

EVANGELINOS, C., LUCOR, D. & KARNIADAKIS, G. E. 2000 DNS-derived force distribution on flexible cylinders subject to vortex-induced vibration. *Journal of Fluids and Structures* **14,** 429–440.

GERRARD, J. H. 1961 An experimental investigation of the oscillating lift and drag of a circular cylinder shedding turbulent vortices. *Journal of Fluid Mechanics* **11,** 244–265.

JADIC, I., SO, R. M. C. & MIGNOLET, M. P. 1998 Analysis of fluid–structure interactions using a time marching technique. *Journal of Fluids and Structures* **12,** 631–654.

KHALAK, A. & WILLIAMSON, C. H. K. 1996 Dynamics of a hydroelastic cylinder with very low mass and damping. *Journal of Fluids and Structures* **10,** 455–472.

LAM, K. & CHAN, Y. F. 1998 A refined surface vorticity modelling method for separated flow around a circular cylinder. *Proceedings of the 1998 ASME Fluids Engineering Division Summer Meeting*, FED-Vol. 245, Session 191-03, FEDSM98-5199, Washington, DC 21–23 June.

LEWIS, R. I. 1991 Surface vorticity modelling of separated flows from two-dimensional bluff bodies of arbitrary shape. *Journal of Mechanical Engineering Science* **23,** 1–12.

MARPLE JR., S. L. 1987 *Digital Spectral Analysis with Applications*. Englewood Cliffs, NJ: Prentice–Hall.

MENDES, P. A. & BRANCO, F. A. 1999 Analysis of fluid–structure interaction by an arbitrary Lagrangian–Eulerian finite element formulation. *International Journal for Numerical Methods in Fluids* **30,** 897–919.

MIGNOLET, M. P. & RED-HORSE, J. R. 1994 ARMAX identification of vibrating structures: model and model order determination. *Proceedings of the 35th Structures, Structural Dynamics, and Materials* Conference, Hilton Head, South Carolina, April 18–20, pp. 1628–1637.

MITTAL, S. & KUMAR, V. 1999 Finite element study of vortex-induced cross-flow and in-line oscillations of a circular cylinder at low Reynolds numbers. *International Journal for Numerical Methods in Fluids* **31,** 1087–1120.

NEWMAN, D. J. & KARNIADAKIS, G. 1997 A direct numerical simulation study of flow past a freely vibrating cable. *Journal of Fluid Mechanics* **344,** 95–136.

RICHTER, A. & NAUDASCHER, E. 1976 Fluctuating forces on a rigid circular cylinder in a confined flow. *Journal of Fluid Mechanics* **78,** 561–576.

ROSHKO, A. 1954 On the development of turbulent wakes from vortex streets, NACA Report 1191.
SCHLICHTING, H. 1968 *Boundary-Layer Theory*, 6th edition, New York: McGraw-Hill.
SO, R. M. C. & SAVKAR, S. D. 1981 Buffeting forces on rigid circular cylinders in cross flows. *Journal of Fluid Mechanics* **105,** 397–425.
SO, R. M. C., JADIC, I. & MIGNOLET, M. P. 1999 Fluid–structure resonance produced by oncoming alternating vortices. *Journal of Fluids and Structures* **13,** 519–548.
SO, R. M. C., ZHOU, Y. & LIU, M. H. 2000 Free vibrations of an elastic cylinder in a cross flow and their effects on the near wake. *Experiments in Fluids* **29,** 130–144.
STOKES, N. 1994 Manual of Fastflo, Ver. 2, CSIRO, Australia.
SZEPESSY, S. & BEARMAN, P. W. 1992 Aspect ratio and end plate effects on vortex shedding from a circular cylinder. *Journal of Fluid Mechanics* **234,** 191–217.
ZDRAVKOVICH, M. M. 1997 *Flow Around Circular Cylinders*, pp. 90, 106. Oxford: Oxford University Press.
ZHOU, C. Y., SO, R. M. C. & LAM, K. 1999 Vortex-induced vibrations of elastic circular cylinders. *Journal of Fluids and Structures* **13,** 165–189.
ZHOU, C. Y., SO, R. M. C. & MIGNOLET, M. P. 2000 Fluid damping of an elastic cylinder in a cross flow. *Journal of Fluids and Structures* **14,** 303–322.